Electronic Supplementary Material (ESI) for Journal of Materials Chemistry A.

Electronic supporting information for

Methanol-assisted energy-saving green hydrogen production using electrodeposited 3D-metallic tin as electrocatalyst

Aparna Sajeev[1], Karthikeyan Krishnamoorthy[1], Parthiban Pazhamalai[1], Kousik Bhunia[1] ,
Arunprasath Sathyaseelan[1] and Sang-Jae Kim[1,2,3,*]

[1]Nanomaterials & System Laboratory, Major of Mechatronics Engineering, Faculty of Applied Energy System, Jeju National University, Jeju, 63243, South Korea

[2]Department of Physics, School of Advanced Sciences, Vellore Institute of Technology, Vellore, 632014, India

[3]Research Institute of New Energy Industry (RINEI), Jeju National University, Jeju, 63243, South Korea.

[4]Nanomaterials & System Lab, Major of Mechanical System Engineering, College of Engineering, Jeju National University, Jeju, 63243, South Korea

*Corresponsding Email id.: kimsangj@jejunu.ac.kr

S1. Experimental section

S1.1. Materials and chemicals

All chemicals used in this were of an analytical grade without further purification. Tin chloride ($SnCl_2$), sodium citrate ($Na_3C_6H_5O_7$), Sulfuric acid (H_2SO_4), Methanol (CH_3OH) and Potassium hydroxide (KOH) were procured from Daejung Chemicals Ltd., South Korea. The nickel foam (NF) (thickness 1.7 mm) substrate was purchased from Heze Jiaotong Xinda Import and Export Co., Ltd.

S1.2. Preparation of binder free 3D metallic Sn on nickel foam (NF)

A facile one-step method was used to prepare Sn on NF via the electrodeposition method. Prior to electrodeposition, the Ni foam (1×1 cm^2) was cleaned using dilute HCl followed by acetone and deionized water (DI) via a sonication process to remove the dust and native surface oxide layer. According to the literature report [1], the electrodeposition process was followed with some modifications. Briefly, the electrolyte for Sn grown on NF substrate was prepared by $SnCl_2$ (18 mM) dissolved in $Na_3C_6H_5O_7$ (50 mM) solution, and the pH of the solution was adjusted to 6 by adding H_2SO_4. The solution was stirred using a magnetic stirrer until the solution became transparent. The electrodeposition process was carried out in a 3-electrode setup using Ag/AgCl, Pt sheet and NF as a reference, counter and working electrode, respectively. The electrodes were immersed in the above-prepared electrolyte solution. The electrodeposition process was carried out using the chronoamperometry technique by applying a potential of -1.1 V for 5, 10, and 15 min., and the samples were labeled as 3D Sn/NF-5, 3D Sn/NF-10 and 3D Sn/NF-15 respectively. After the electrodeposition process, each electrode was rinsed with ethanol and placed in a vacuum oven at 70°C for 12 h.

S1.3. Characterization

The phase purity and crystallinity of Sn deposited on NF for various time intervals were analyzed using an X-ray diffraction pattern (XRD) on an Empyrean X-ray diffractometer (Malvern Panalytical, UK) equipped with Cu-Kα radiation ($\lambda = 1.54184$ Å). The surface morphology and elemental mapping of Sn deposited on NF for various time intervals were characterized using a field-emission scanning electron microscope (TESCAN, MIRA3) coupled with an energy-dispersive x-ray spectroscopy (EDS) analyzer. The surface composition/electronic state of elements in Sn deposited on NF were analyzed via X-ray photoelectron spectroscopy (XPS) analysis using an ESCA-2000 (VG Microtech Ltd) at Korea Basic Science Institute (KBSI), Busan.

S1.4. Electrochemical characterization

The electrochemical hydrogen evolution reaction (HER), oxygen evolution reaction (OER) and Methanol oxidation reaction (MOR) three-electrode activities were characterized using the Auto lab PGSTAT302N electrochemical workstation. All electrochemical investigations were carried out at room temperature. The as-prepared Sn deposited on NF (1×1 cm^2), Ag/AgCl and Pt sheet were used as the working electrodes, reference and counter electrode, respectively, for 3 electrode investigation. All the potentials were corrected to a reversible hydrogen electrode (RHE) by using the following equation:

$$E_{(RHE)} = E_{(Ag/AgCl)} + 0.059pH + E^0_{(Ag/AgCl)} \text{ --------------------- } (1)$$

All the current densities were normalized to the geometric area of NF. Cyclic voltammetry (CV) and Linear sweep voltammetry (LSV) curves were carried out in 1 M KOH with and without different concentrations of CH_3OH at a scan rate of 50 mV s^{-1} and 5 mV s$^{-1,}$ respectively, unless specified. Chronopotentiometry and chronoamperometry were used to analyze the stability of the catalyst. The electrochemical impedance spectroscopy (EIS) was carried out at an open circuit voltage of 0V and by applying -0.14, 1.5 and 1.4 V for HER, OER and MOR, respectively, recorded from 100 kHz to 0.1 Hz with an amplitude of 5 mV. The electrochemical active surface area (ECSA) of electrodeposited samples was calculated from CV in the potential range of 0.82 to 0.92 V in various scan rates of 20, 40, 60, 80 and 100 mV s^{-1}.

$$\mathrm{ECSA} = \frac{Cdl}{Cs} \qquad \text{---------------------------- (2)}$$

C_{dl} is double-layer capacitance calculated from the slope of current density (at 0.88 V) plotted against scan rates. The Cs value is taken as 40 µF cm^{-2}. The two electrode measurements were carried out using the same electrode in the anode and cathode in 1 M KOH containing different concentrations of CH_3OH. Stability analysis of the device was performed by using chronopotentiometry at 10 mA cm^{-2} for 12 h in 1 M KOH containing 1 M CH_3OH. All the polarization curves are with 100% iR correction.

S2. Mechanism of MOR

The mechanism of methanol oxidation reaction (MOR) starts with the adsorption of methanol on to the surface of the catalyst and the reaction proceeds with multiple steps of reaction which results in the formation of formate.[2]

$OH^- + Sn \rightarrow Sn/Sn(OH)_{2\ surf}$ ---------------- (1)

$OH^- + Sn/Sn(OH)_{2\ surf} \rightarrow Sn/Sn(OOH)_{surf} + H_2O + e^-$ ---------------- (2)

$CH_3OH_{sol} \rightarrow CH_3OH_{ads}$ ---------------- (3)

$CH_3OH_{ads} + Sn/Sn(OOH)_{surf} \rightarrow C^*H_2OH + Sn/Sn(OH)_{2\ surf}$ ---------------- (4)

$C^*H_2OH + 3Sn/Sn(OOH)_{surf} + OH^- \rightarrow CHOO^- + 3\ Sn/Sn(OH)_{2\ surf}$ ---------------- (5)

The overall reaction:

$CH_3OH + 5OH^- \rightarrow HCOO^- + 4H_2O + 4e^-$ ---------------- (6)

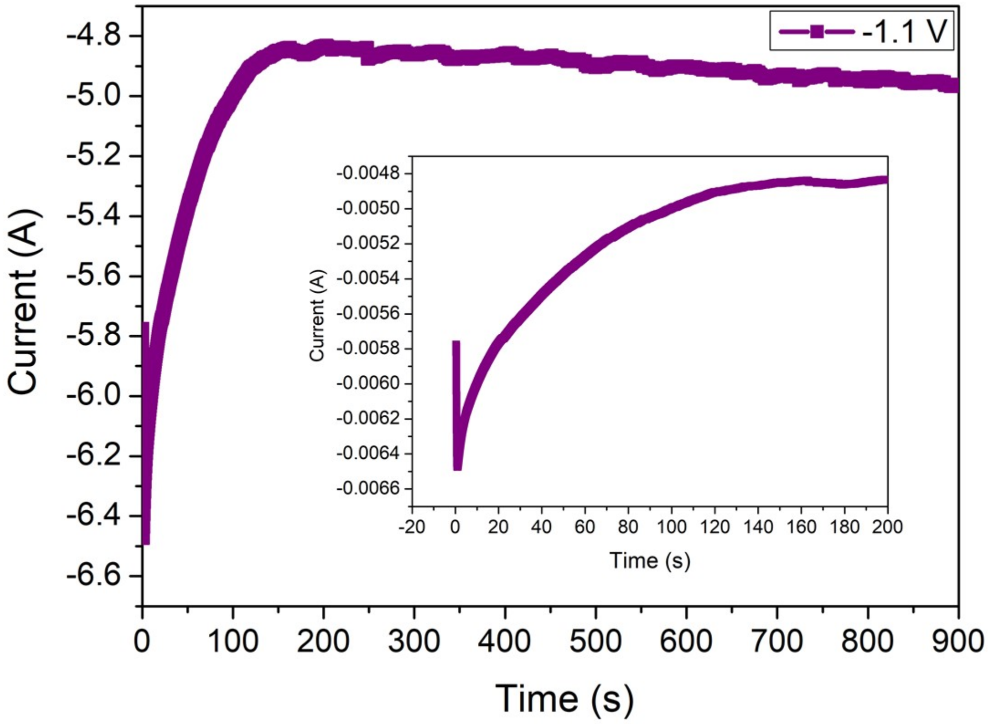

Figure S1. Electrochemical deposition profile for 3-D Metallic Sn on NF (3D Sn/NF-15.)

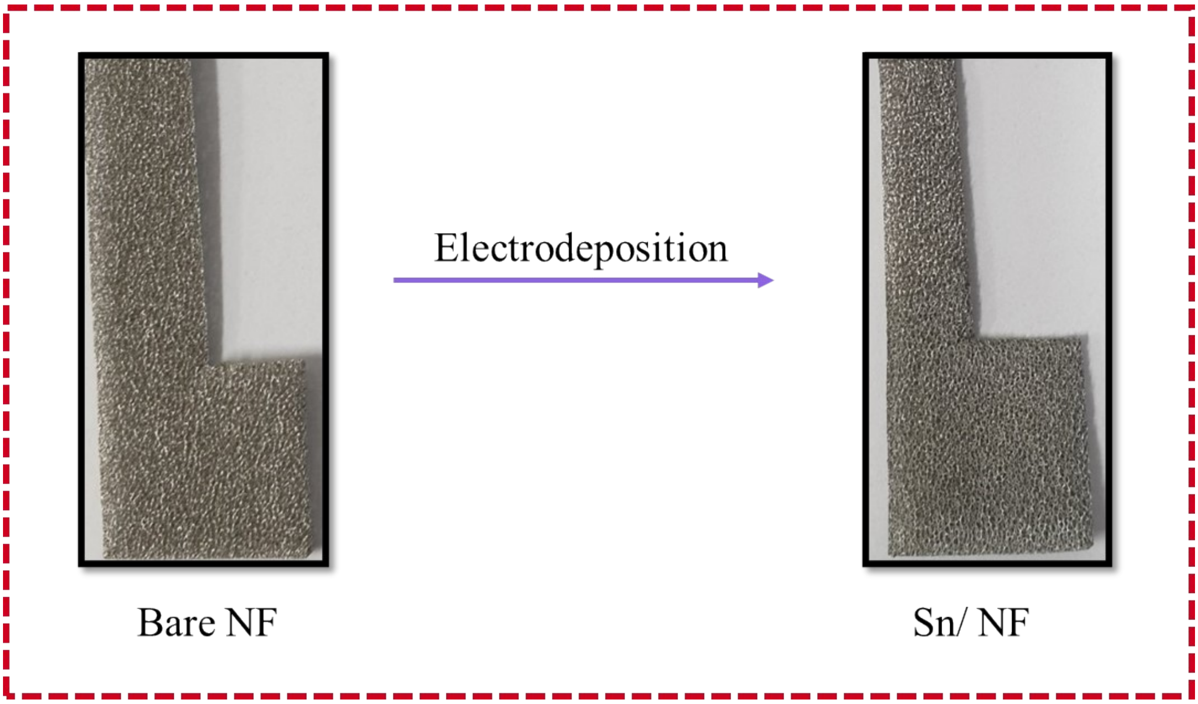

Figure S2. Digital image of bare NF and electrodeposited Sn/NF

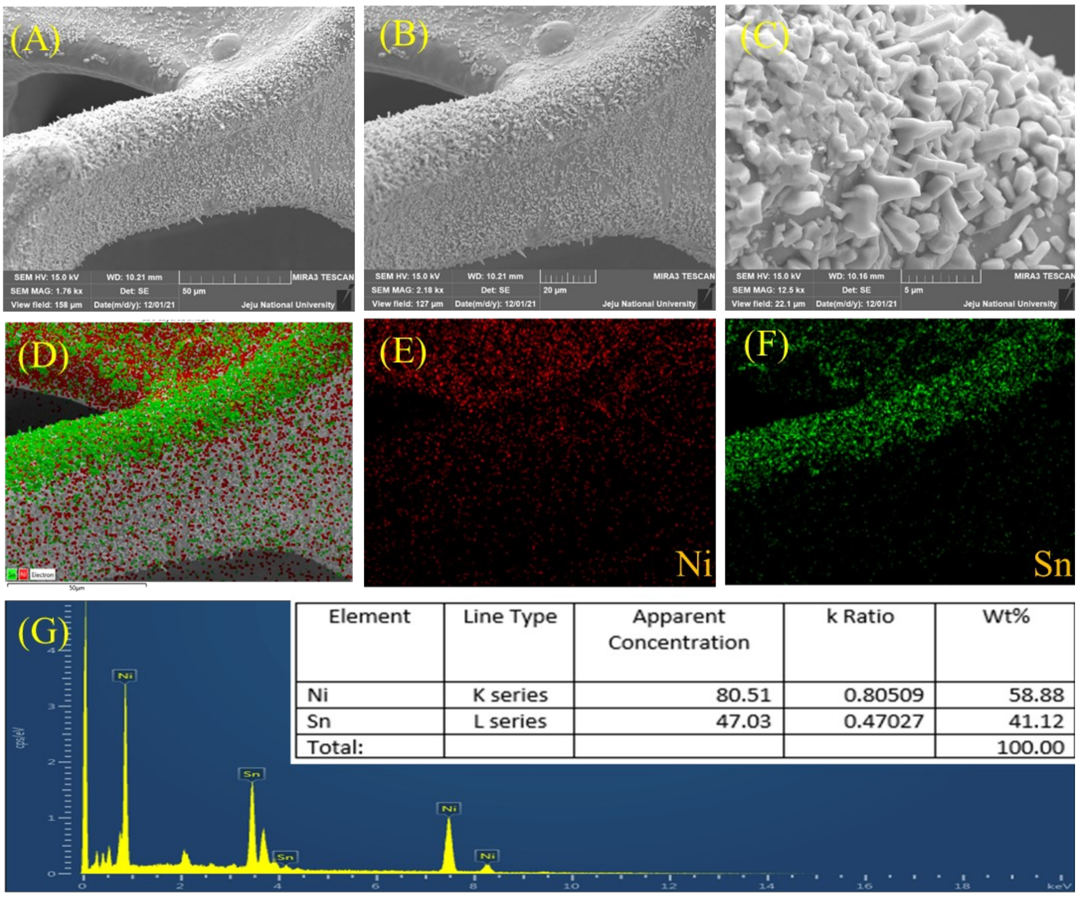

Element	Line Type	Apparent Concentration	k Ratio	Wt%
Ni	K series	80.51	0.80509	58.88
Sn	L series	47.03	0.47027	41.12
Total:				100.00

Figure S3. FE-SEM image of (A-C) 3D Sn/NF-5 at various magnification, (D) overlay map of 3D Sn/NF-5 (E-F) elemental mapping of Ni, Sn present in 3D Sn/NF-5 (G) energy dispersive X-ray spectrum of 3D Sn/NF-5

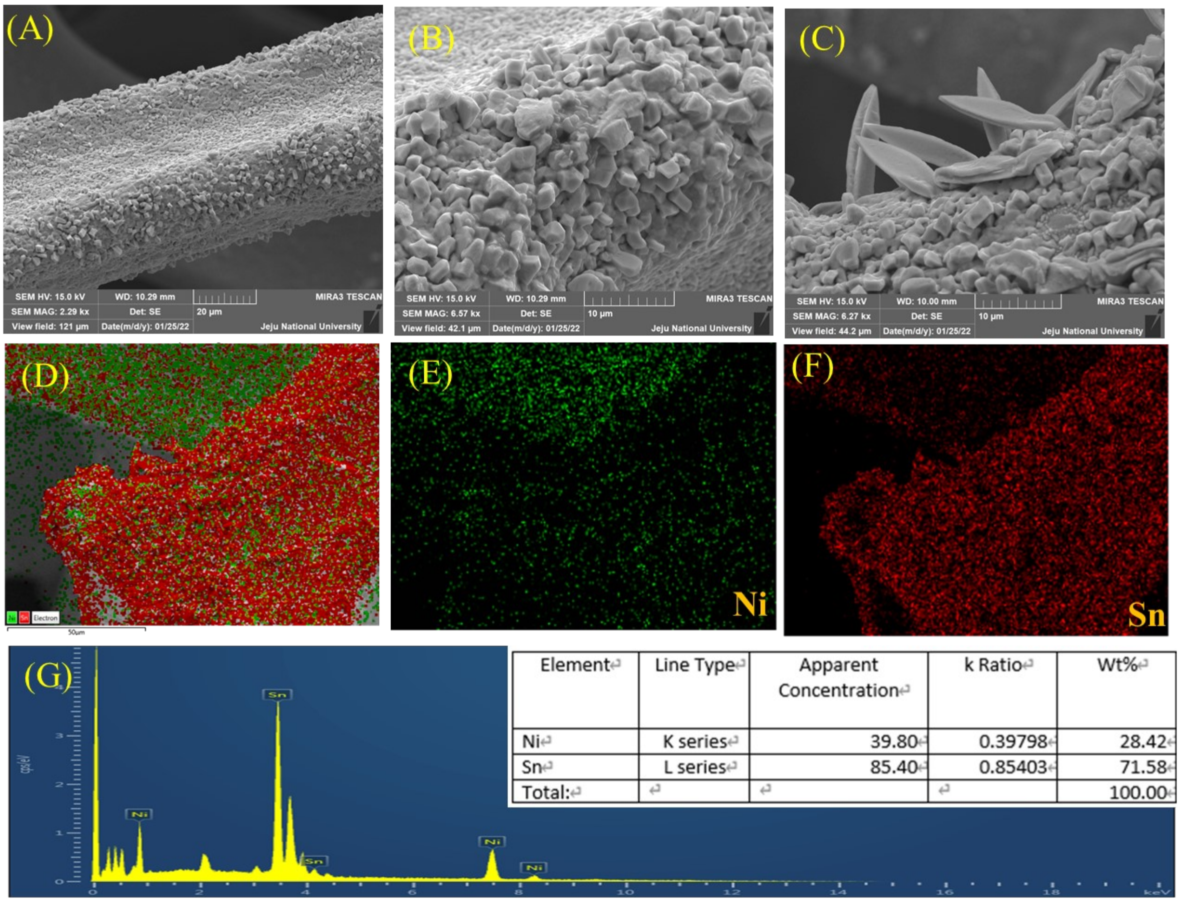

Element	Line Type	Apparent Concentration	k Ratio	Wt%
Ni	K series	39.80	0.39798	28.42
Sn	L series	85.40	0.85403	71.58
Total:				100.00

Figure S4. FE-SEM image of (A-C) 3D Sn/NF-10 at various magnifications, (D) overlay map of 3D Sn/NF-10 (E-F) elemental mapping of Ni, Sn present in 3D Sn/NF-10 (G) energy dispersive X-ray spectrum of 3D Sn/NF-10

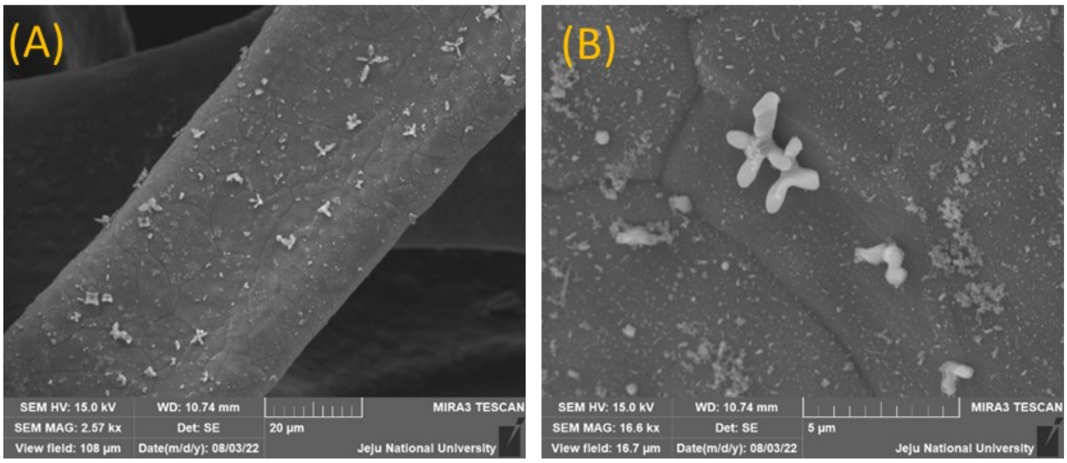

Figure S5. FE-SEM image of (A-B) Electrodeposited Sn in the absence of sodium citrate at various magnification

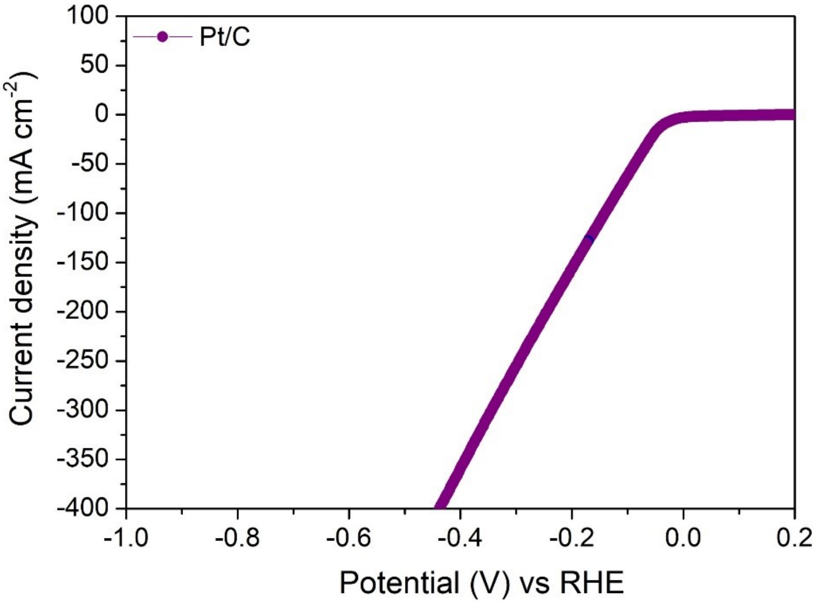

Figure S6. HER polarization curve for Pt/C/NF in 1 M KOH

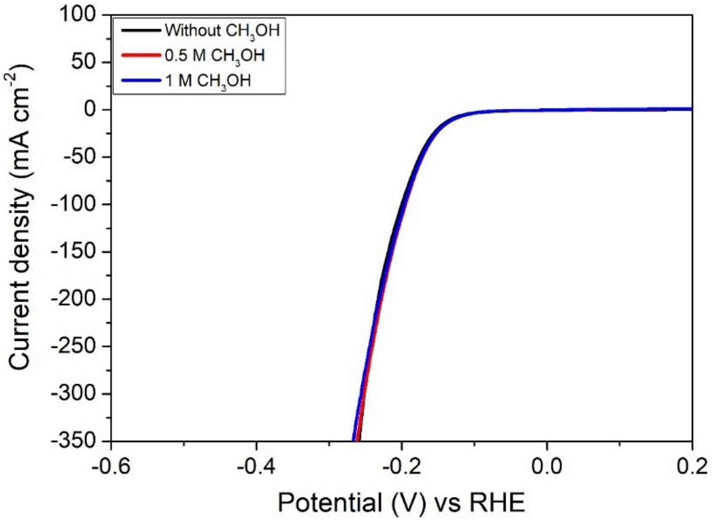

Figure S7. HER polarization curve for 3D Sn/NF-15 in 1 M KOH with and without CH_3OH

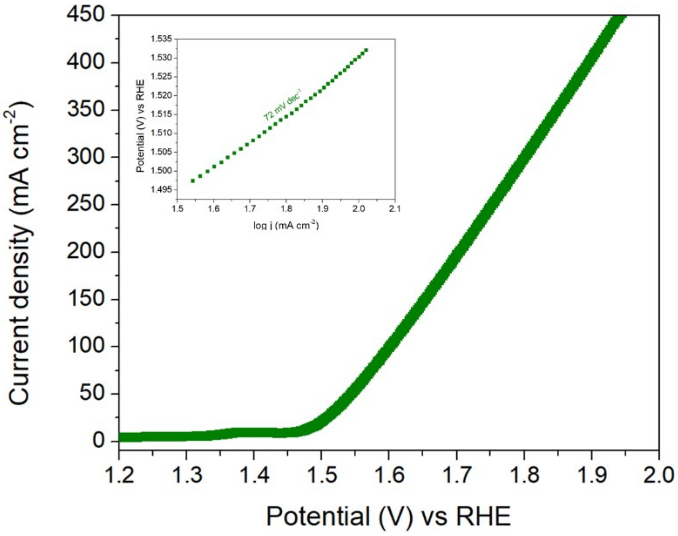

Figure S8. OER polarization curve for IrO_2/NF in 1 M KOH

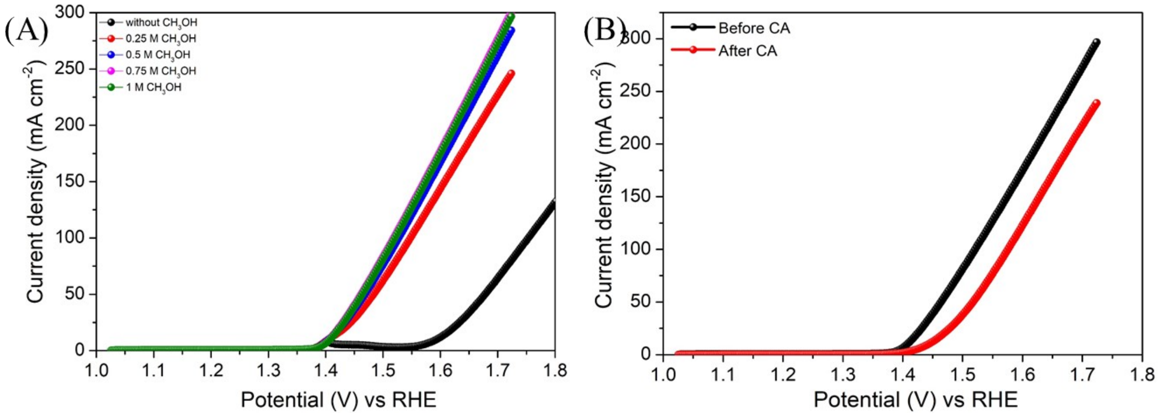

Figure S9. Electrochemical performance of 3D Sn/NF-5 towards MOR. (A) CV of 3D Sn/NF-5 at various scan rates in 1 M KOH (B) CV of 3D Sn/NF-5 at a scan rate of 50 mV s^{-1} in 1 M KOH with different concentrations of CH_3OH. (C) LSV of 3D Sn/NF-5 at a scan rate of 5 mV s^{-1} in 1 M KOH with varying concentrations of CH_3OH. (D) LSV of 3D Sn/NF-5 at a scan rate of 5 mV s^{-1} in 1 M KOH containing 1 M CH_3OH before and after CA.

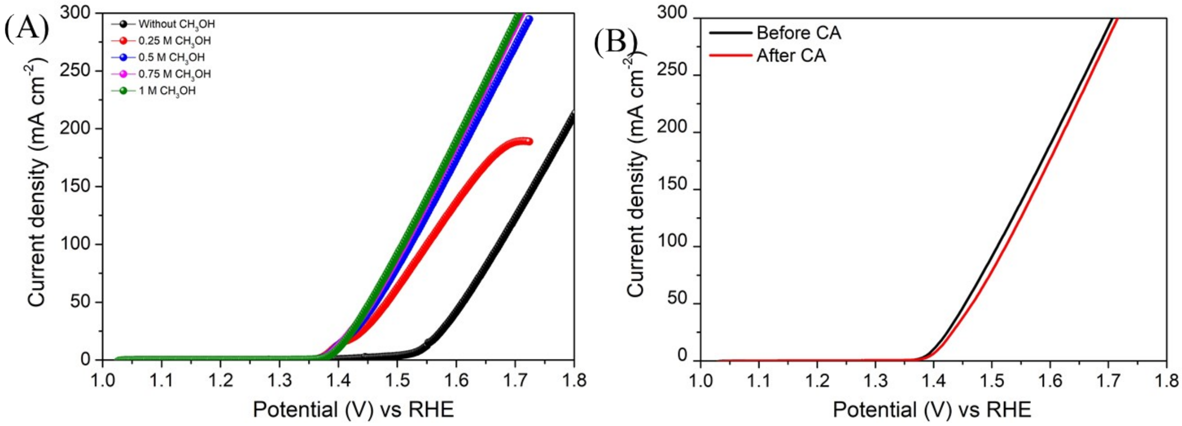

Figure S10. Electrochemical performance of 3D Sn/NF-10 towards MOR. (A) CV of 3D Sn/NF-10 at various scan rates in 1 M KOH (B) CV of 3D Sn/NF-10 at a scan rate of 50 mV s^{-1} in 1 M KOH with different concentrations of CH_3OH. (C) LSV of 3D Sn/NF-10 at a scan rate of 5 mV s^{-1} in 1 M KOH with varying concentrations of CH_3OH. (D) LSV of 3D Sn/NF-10 at a scan rate of 5 mV s^{-1} in 1 M KOH containing 1 M CH_3OH before and after CA.

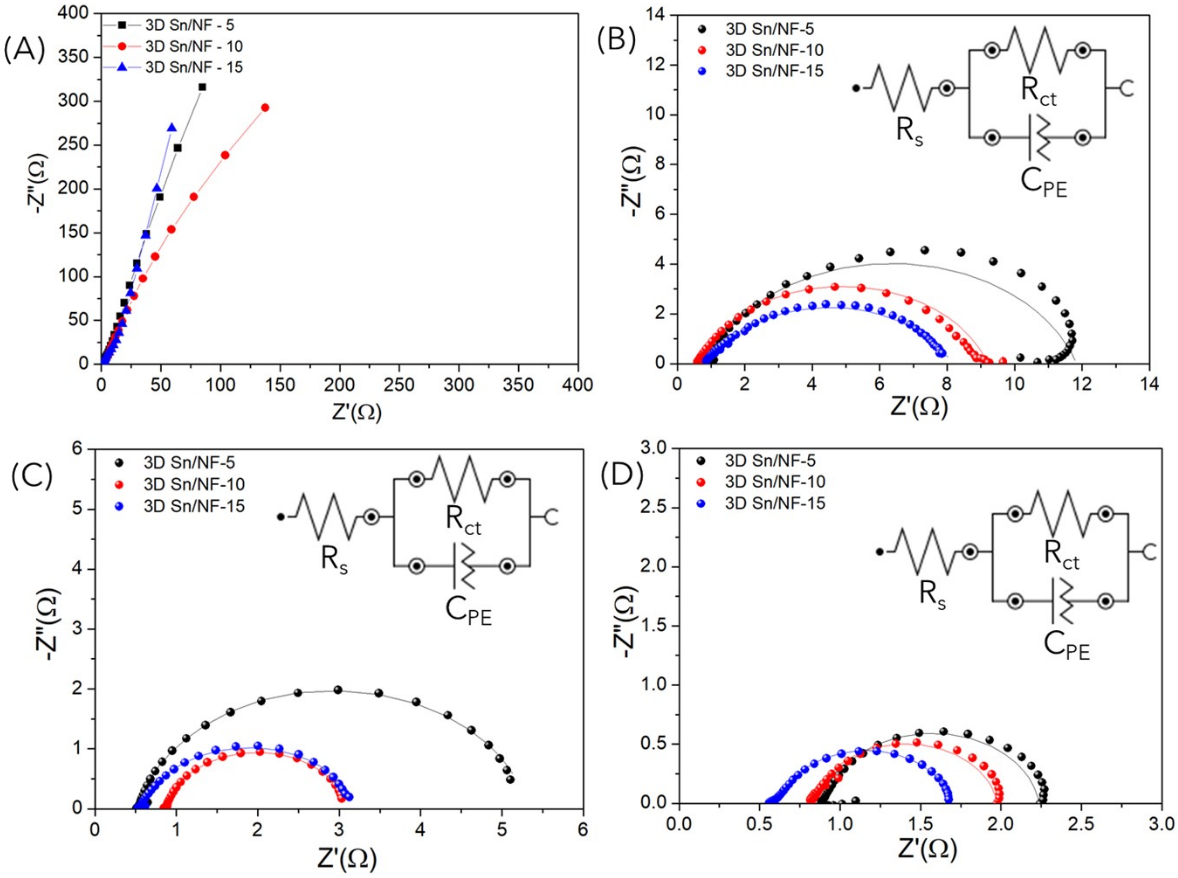

Figure S11. Electrochemical impedance spectra of various catalysts in 1.0 M KOH with different applied potentials: (A) 0 V (vs. RHE), (B) -0.147 V (vs. RHE) for HER, (C) 1.52 V (vs. RHE) for OER, (D) 1.42 V (vs. RHE) with 1 M CH_3OH in 1 M KOH for MOR.

The potential of -0.147 V (vs. RHE), 1.52 V (vs. RHE) and 1.42 V (vs. RHE) is chosen to analyze the kinetics of electrodes of all samples towards the HER, OER and MOR, respectively. Here, Rs, Rct, and C_{PE} represent solution resistance, charge transfer resistance, electrode and constant phase element, respectively.

Table S1: Lists of elements and corresponding values from the equivalent circuit fitting for Nyquist plot measured at -0.147 V vs. RHE (HER), 1.52 V vs. RHE (OER), 1.42 V vs. RHE (MOR)

	HER		OER		MOR	
Electrode	**Rs**	**Rct**	**Rs**	**Rct**	**Rs**	**Rct**
3D Sn/NF-5	0.897	10.9	0.530	4.80	0.910	1.32
3D Sn/NF-10	0.604	8.59	0.869	2.24	0.843	1.24
3D Sn/NF-15	0.871	7.28	0.553	2.56	0.552	1.14

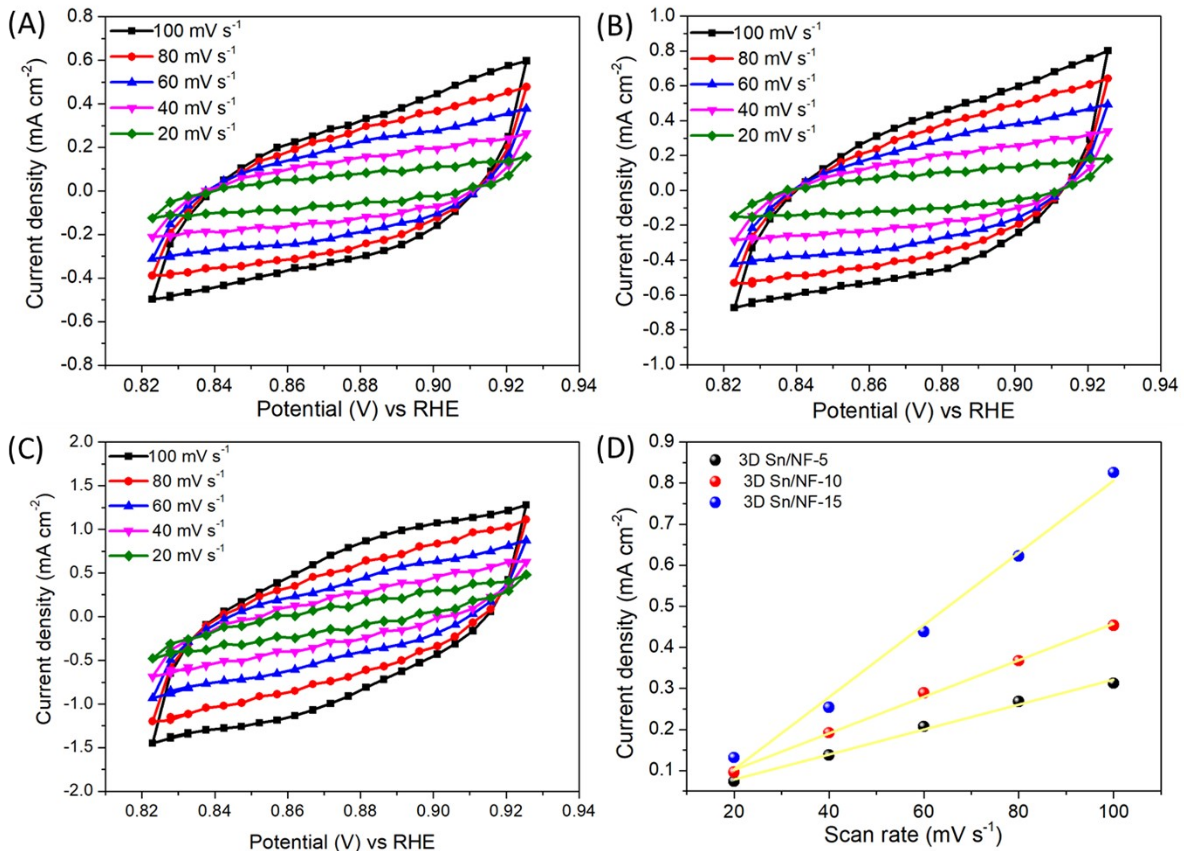

Figure S12. Electrochemical double-layer capacitance measurements of (A) 3D Sn/NF-5, (B) 3D Sn/NF-10 and (C) 3D Sn/NF-15 at scan rates of 20, 40, 60, 80 and 100mV s^{-1} (D) The plot of scan rate vs. current density of various time interval deposited 3D Metallic Sn at 0.88 V.

Calculation for Turnover Frequency (TOF)

TOF per active site can be calculated by the following equation

$$TOF_{per\ site} = \frac{the\ \ number\ of\ total\ hydrogen\ turn\ overs}{the\ number\ of\ surface\ active\ sites}$$

$$TOF = \frac{j \times N_A}{n \times F \times \Gamma}$$

Where j is current density at specific overpotential; N_A is Avogadro constant; n is the number of charge transfer (2 for HER and 4 for OER); F is Faradaic constant; Γ is the number of surface-active sites.[3]

The number of surface-active sites of 3D Sn/NF-15 per $cm^2 = 2.354\ x\ 10^{17}$

Table S2. TOF calculated for the prepared catalysts.

Electrocatalyst	**TOF @250 mV for HER**	**TOF @360mV for OER**
3D Sn/NF-5	4.16 H_2/s	0.303 O_2/s
3D Sn/NF-10	4.56 H_2/s	1.36 O_2/s
3D Sn/NF-15	4.77 H_2/s	1.56 O_2/s

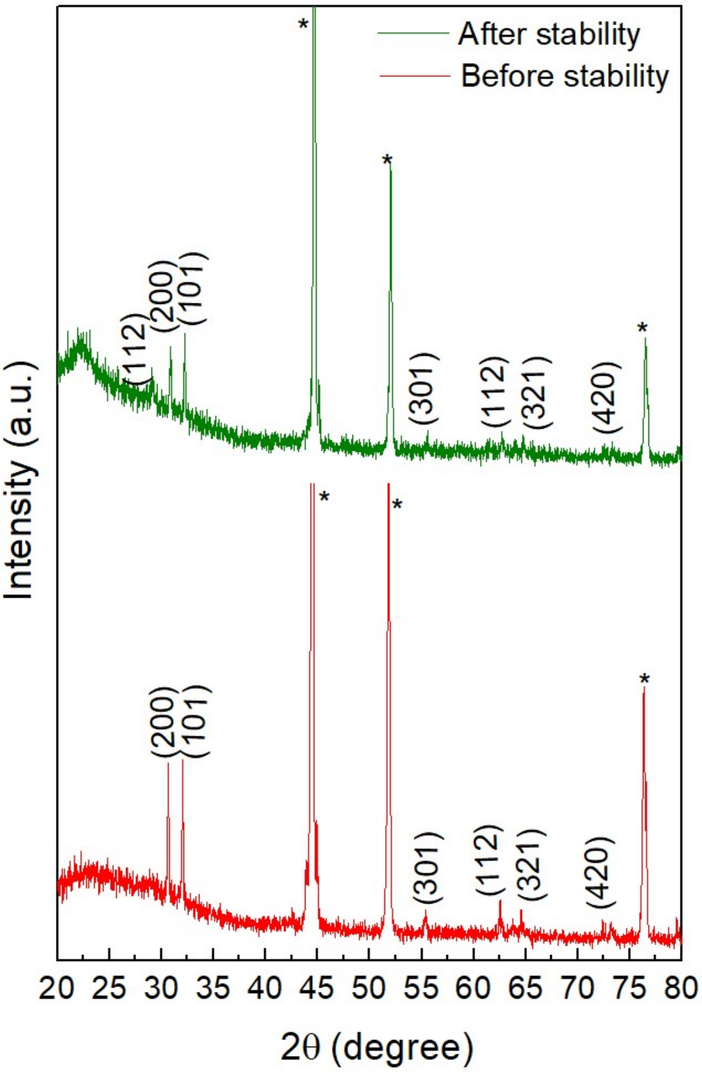

Figure S13. XRD analysis of (A) 3D Sn/NF-15 after post-analysis.

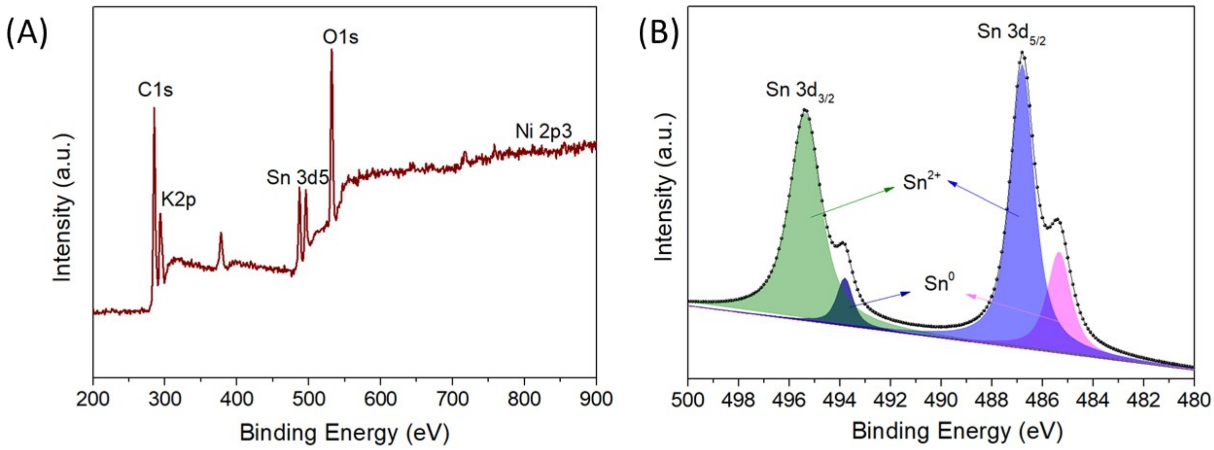

Figure S14. XPS analysis of (A) 3D Sn/NF-15 after post-analysis

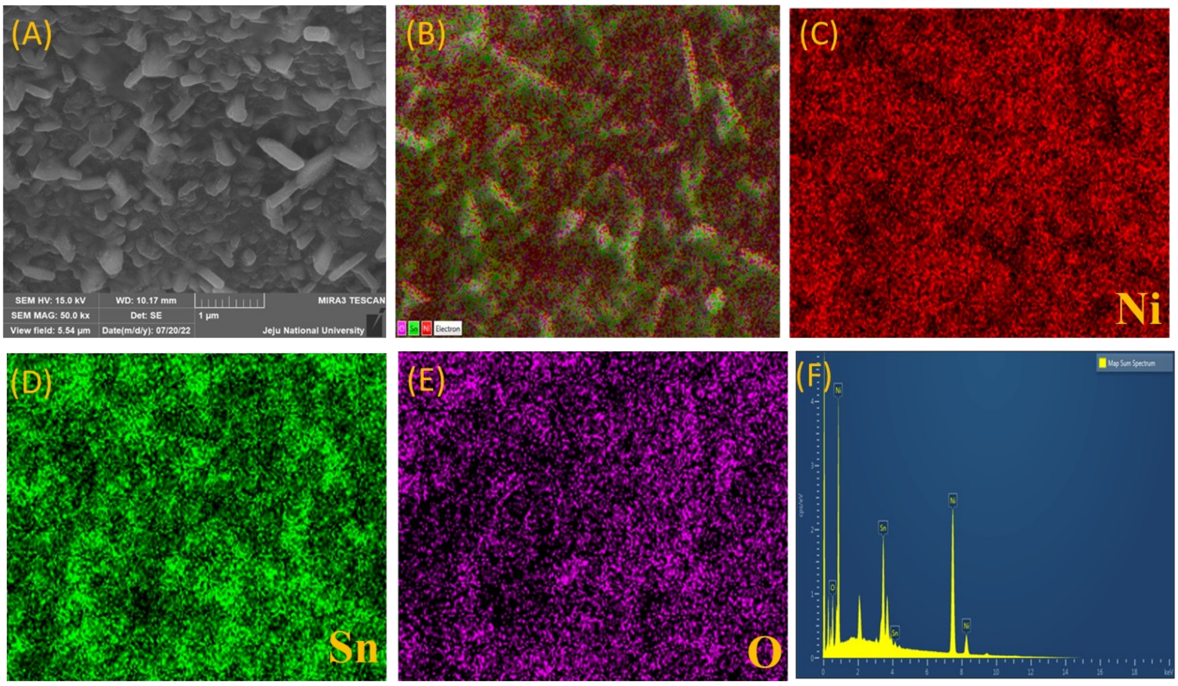

Figure S15. FE-SEM image of (A) 3D Sn/NF-15 after post analysis, (B) overlay map of 3D Sn/NF-15 after post analysis (E-F) elemental mapping of Ni, Sn, O present in 3D Sn/NF-15 after post-analysis (G) energy dispersive X-ray spectrum of 3D Sn/NF-15 after post-analysis

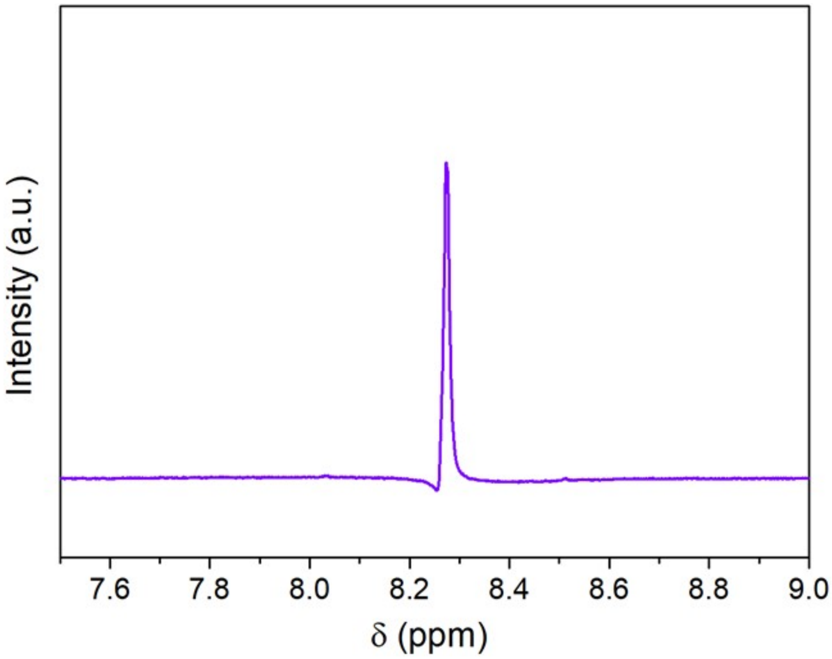

Figure S16. 1H NMR analysis of anodic formate production after chronopotentiometry analysis.

Table S3. Comparison table of electrocatalyst towards HER

S. No	**Electrocatalyst**	**Electrolyte**	**Overpotential (mV)@10 mA cm^{-2}**	**Tafel slope (mV /dec)**	**Ref**
1	Mo-doped NiCo	0.1 M KOH	132	108	[4]
2	$Co(OH)_2$@HOS/CP	1 M KOH	148	109	[5]
3	Co-SP/CC	1 M KOH	167	86	[6]
4	CMS/Ni	1 M KOH	213@50 mA cm^{-2}	80	[7]
5	$Co(OH)_2$@P-NiCo-LDH	1 M KOH	226	134	[8]
6	$NiCo_2O_4$	1 M KOH	156	135	[9]
7	$NiCo_2Se_4/NiCoS_4$	1 M KOH	180	107.4	[10]
8	antimonene	1 M KOH	335	151	[11]
9	Ni-GF/VC	1 M KOH	128	80	[12]
10	3D Sn /NF-15	1 M KOH	127	97	This work

Table S4: Comparative table for the HER performance over other reported metallic alloys

S. No	Electrocatalyst	Electrolyte	Current density (mA cm^{-2})	Overpotential (mV)	Tafel slope (mV dec^{-1})	Ref
1	Mo-doped NiCo	0.1 M KOH	10	132	108	4
2	$Cr_{15}Fe_{20}Co_{35}Ni_{20}Mo_{10}$	1 M KOH	10	193	89	13
3	AlNiCoIrMo	1 M KOH	10	233	86	
4	CuAlNiMoFe	1 M KOH	50	310	124	14
5	V1.0CuCoNiFeMn	1 M KOH	50	250	134	15
6	CoZnCdCuMnS@CF	1 M KOH	10	173	-	16
7	Ni-Co	1 M KOH	20	142	120	17
8	CoFeLaNiPt	0.1 M KOH	10	536	311	18
9	TiNbTaCrMo	1 M KOH	50	970	96.33	19
10	NiCoFeMnCrP	1.0 M KOH	10	220	94.5	20
11	3D Sn /NF-15	1 M KOH	10	127	97	This work

Table S5: Comparative table for the OER performance over other reported metallic alloys

S. No	Electrocatalyst	Electrolyte	Current density (mA cm^{-2})	Overpotential (mV))	Tafel slope (mV /dec)	Ref
1	FeCoNiMoCr	1 M KOH	10	360	73.45	[21]
2	FeCoNiMnW	H2SO4	10	512	92.2	[22]
3	IrNiTa	1 M KOH	10	278	40	[23]
4	FeCoNiCrMn	1 M KOH	50	345 mV	81.3	[24]
5	Fe$_{0.5}$CoNiCuZn$_{0.8}$	1 M KOH	10	340 mV	62	[25]
6	CoFeGaNiZn	1 M KOH	10	370	136.7	[26]
7	FeCoNiCuCr	1.0 M NaOH	10	330	80	[27]
8	FeNiMnCrCu	1.0 M NaOH	10	314	58	[28]
9	3D Sn /NF-15	1 M KOH	10	310	87	This work

Table S6. Comparison table of electrocatalyst towards OER

S. No	**Electrocatalyst**	**Electrolyte**	**Overpotential (mV) @10 mA cm^{-2}**	**Tafel slope (mV /dec)**	**References**
1	NiCo foam	1 M KOH	340	165	[29]
2	$NiCo_2O_4$	1 M KOH	320	92.2	[9]
3	$NiCo_2Se_4/NiCoS_4$	1 M KOH	248	98.5	[10]
4	CMS/Ni	1 M KOH	350@50 mA cm^{-2}	124	[7]
5	$Ni1Co_3$@BC	1 M KOH	309	62	[30]
6	Cu_2Se	1 M KOH	290	136.7	[31]
7	Ir/C	1 M KOH	380	50	[32]
8	NiO/NF	1 M KOH	280	200	[33]
9	3D Sn /NF-15	1 M KOH	310	87	This work

Table S7. Comparison table of electrocatalyst towards MOR

S. No	Electrocatalyst	Electrolyte	Potential (V) @10 mA cm^{-2}	Tafel slope (mV /dec)	Ref
1	$Co(OH)_2$@HOS/CP	1 M KOH + 1M CH_3OH	1.39	71	[5]
2	Ni-MOF/NF	1 M KOH + 4 M CH_3OH	1.39	52.5	[34]
3	RuO_2/NF	1 M KOH + 4 M CH_3OH	1.36	90.5	[34]
4	NiCoO-400	1 M KOH + 1M CH_3OH	1.4	145	[35]
5	NiO/NF	1 M KOH + 1M CH_3OH	1.38	135	[33]
6	NiS/NF	1 M KOH + 1M CH_3OH	1.36	25	[36]
7	$Ni_{1.7}Sn$ NPs/CB	0.5 M KOH + 0.5 M CH_3OH	1.48	-	[37]
8	$Ni_{2.5}Co_{0.5}Sn_2$ NPs	1 M KOH + 1M CH_3OH	1.45	–	[38]
9	NiFe NPs	1 M NaOH + 1M CH_3OH	1.53	–	[39]
10	3D Sn /NF-15	1 M KOH + 1M CH_3OH	1.39	51	This work

Table S8. Comparison of cell voltage of alcohol oxidation-assisted water electrolyzers.

S. No	Bifunctional Electrocatalyst	Electrolyte	Current density	Cell voltage	Ref
1	α-$Co(OH)_2$/CP	1 M KOH + 3M Methanol	10	1.758	[5]
2	Ni_2P/NF	1.M KOH+10 mM HMF	10	1.65	[40]
3	Co-S-P/CC	1 M KOH + 1 M Ethanol	10	1.63	[6]
4	$CoS_x(OH)_y$/CP	1 M KOH + 3M Methanol	10	1.578	[5]
5	NC@$CuCo_2N_x$/CF	1 M KOH + 0.015 M benzyl alcohol	10	1.55	[41]
6	Ni $(OH)_2$/NF	1 M KOH + 0.5 M methanol	10	1.52	[42]
7	$Ni_{0.33}Co_{0.67}(OH)_2$/NF	1 M KOH + 0.5 methanol	10	1.50	[43]
8	3D Sn /NF-15	1 M KOH + 1 M Methanol	10	1.54	This work

References

1 X. An, S. Li, A. Yoshida, Z. Wang, X. Hao, A. Abudula and G. Guan, *ACS Sustain Chem Eng*, 2019, **7**, 9360–9368.

2 Y. Yi, J. Li and C. Cui, *Chinese Chemical Letters*, 2022, **33**, 1006–1010.

3 C. T. Hsieh, C. L. Huang, Y. A. Chen and S. Y. Lu, *Appl Catal B*, 2020, **267**, 118376.

4 D. Gao, J. Guo, X. Cui, L. Yang, Y. Yang, H. He, P. Xiao and Y. Zhang, *ACS Appl Mater Interfaces*, 2017, **9**, 22420–22431.

5 K. Xiang, D. Wu, X. Deng, M. Li, S. Chen, P. Hao, X. Guo, J. L. Luo and X. Z. Fu, *Adv Funct Mater*, , DOI:10.1002/adfm.201909610.

6 S. Sheng, K. Ye, L. Sha, K. Zhu, Y. Gao, J. Yan, G. Wang and D. Cao, *Inorg Chem Front*, 2020, **7**, 4498–4506.

7 A. Sajeev, V. K. Mariappan, D. Kesavan, K. Krishnamoorthy and S. J. Kim, *Mater Adv*, 2021, **2**, 455–463.

8 N. Song, S. Hong, M. Xiao, Y. Zuo, E. Jiang, C. Li and H. Dong, *J Colloid Interface Sci*, 2021, **582**, 535–542.

9 B. Zhang, X. Zhang, Y. Wei, L. Xia, C. Pi, H. Song, Y. Zheng, B. Gao, J. Fu and P. K. Chu, *J Alloys Compd*, 2019, **797**, 1216–1223.

10 K. Wang, Z. Lin, Y. Tang, Z. Tang, C. L. Tao, D. D. Qin and Y. Tian, *Electrochim Acta*, 2021, **368**, 137584.

11 Y. Li, J. Chen, J. Huang, Y. Hou, L. Lei, W. Lin, Y. Lian, X. Zhonghua, H. H. Yang and Z. Wen, *Chemical Communications*, 2019, **55**, 10884–10887.

12

13 G. Zhang, K. Ming, J. Kang, Q. Huang, Z. Zhang, X. Zheng and X. Bi, *Electrochim Acta*, 2018, **279**, 19–23.

14 A. Sivanantham, H. Lee, S. W. Hwang, H. U. Lee, S. B. Cho, B. Ahn and I. S. Cho, *Adv Funct Mater*, 2023, **33**, 2301153.

15 R.-Q. Yao, Y.-T. Zhou, H. Shi, W.-B. Wan, Q.-H. Zhang, L. Gu, Y.-F. Zhu, Z. Wen, X.-Y. Lang, Q. Jiang, R.-Q. Yao, Y.-T. Zhou, H. Shi, W.-B. Wan, Y.-F. Zhu, Z. Wen, -Y X Lang, Q. Jiang, -H Q Zhang and L. Gu, *Adv Funct Mater*, 2021, **31**, 2009613.

16 Y. Lei, L. Zhang, W. Xu, C. Xiong, W. Chen, X. Xiang, B. Zhang and H. Shang, *Nano Res*, 2022, **15**, 6054–6061.

17 G. B. Darband, M. Aliofkhazraei, A. S. Rouhaghdam and M. A. Kiani, *Appl Surf Sci*, 2019, **465**, 846–862.

18 M. W. Glasscott, A. D. Pendergast, S. Goines, A. R. Bishop, A. T. Hoang, C. Renault and J. E. Dick, *Nature Communications 2019 10:1*, 2019, **10**, 1–8.

19 X. Wang, Q. Peng, X. Zhang, X. Lv, X. Wang and Y. Fu, *J Colloid Interface Sci*, 2022, **607**, 1580–1588.

20 D. Lai, Q. Kang, F. Gao and Q. Lu, *J Mater Chem A Mater*, 2021, **9**, 17913–17922.

21 X. Huo, X. Zuo, X. Wang, B. Xing and N. Zhang, *Chem Asian J*, 2023, **18**, e202300456.

22 S. Q. Chang, C. C. Cheng, P. Y. Cheng, C. L. Huang and S. Y. Lu, *Chemical Engineering Journal*, 2022, **446**, 137452.

23 D. Liu, Z. Song, S. Cheng, Y. Wang, A. Saad, S. Deng, J. Shen, X. Huang, X. Cai and P. Tsiakaras, *Chemical Engineering Journal*, 2022, **431**, 134210.

24 H. Li, H. Zhu, S. Sun, J. Hao, Z. Zhu, F. Xu, S. Lu, F. Duan and M. Du, *Chemical Communications*, 2021, **57**, 10027–10030.

25 J. Huang, P. Wang, P. Li, H. Yin and D. Wang, *J Mater Sci Technol*, 2021, **93**, 110–118.

26 L. Sharma, N. K. Katiyar, A. Parui, R. Das, R. Kumar, C. S. Tiwary, A. K. Singh, A. Halder and K. Biswas, *Nano Res*, 2022, **15**, 4799–4806.

27 R. Nandan, M. Y. Rekha, H. R. Devi, C. Srivastava and K. K. Nanda, *Chemical Communications*, 2021, **57**, 611–614.

28 X. Cui, B. Zhang, C. Zeng and S. Guo, *MRS Commun*, 2018, **8**, 1230–1235.

29 F. Arshad, T. ul Haq, A. Khan, Y. Haik, I. Hussain and F. Sher, *Energy Convers Manag*, 2022,

254, 115262.

30 C. Shuai, Z. Mo, X. Niu, Y. Du, Q. Gao, J. Liu, N. Liu and R. Guo, *Appl Surf Sci*, 2020, **532**, 147381.

31 J. Masud, W. P. R. Liyanage, X. Cao, A. Saxena and M. Nath, *ACS Appl Energy Mater*, 2018, **1**, 4075–4083.

32 V. Vij, S. Sultan, A. M. Harzandi, A. Meena, J. N. Tiwari, W. G. Lee, T. Yoon and K. S. Kim, *ACS Catal*, 2017, **7**, 7196–7225.

33 M. I. Abdullah, A. Hameed, N. Zhang, M. H. Islam, M. Ma and B. G. Pollet, *ACS Appl Mater Interfaces*, 2021, **13**, 30603–30613.

34 Y. Xu, M. Liu, M. Wang, T. Ren, K. Ren, Z. Wang, X. Li, L. Wang and H. Wang, *Appl Catal B*, 2022, **300**, 120753.

35 S. Chen, D. Huang, D. Liu, H. Sun, W. Yan, J. Wang, M. Dong, X. Tong and W. Fan, *Appl Catal B*, 2021, **291**, 120065.

36 Z. Pi and H. Zhong, *IOP Conf Ser Earth Environ Sci*, , DOI:10.1088/1755-1315/651/4/042062.

37 J. Li, Z. Luo, Y. Zuo, J. Liu, T. Zhang, P. Tang, J. Arbiol, J. Llorca and A. Cabot, *Appl Catal B*, 2018, **234**, 10–18.

38 J. Li, Z. Luo, F. He, Y. Zuo, C. Zhang, J. Liu, X. Yu, R. Du, T. Zhang, M. F. Infante-Carrió, P. Tang, J. Arbiol, J. Llorca and A. Cabot, *J Mater Chem A Mater*, 2018, **6**, 22915–22924.

39 S. L. Candelaria, N. M. Bedford, T. J. Woehl, N. S. Rentz, A. R. Showalter, S. Pylypenko, B. A. Bunker, S. Lee, B. Reinhart, Y. Ren, S. P. Ertem, E. B. Coughlin, N. A. Sather, J. L. Horan, A. M. Herring and L. F. Greenlee, *ACS Catal*, 2017, **7**, 365–379.

40 B. You, N. Jiang, X. Liu and Y. Sun, *Angewandte Chemie - International Edition*, 2016, **55**, 9913–9917.

41 J. Zheng, X. Chen, X. Zhong, S. Li, T. Liu, G. Zhuang, X. Li, S. Deng, D. Mei and J. G. Wang, *Adv Funct Mater*, 2017, **27**, 1–11.

42 J. Hao, J. Liu, D. Wu, M. Chen, Y. Liang, Q. Wang, L. Wang, X. Z. Fu and J. L. Luo, *Appl Catal B*, 2021, **281**, 119510.

43 M. Li, X. Deng, K. Xiang, Y. Liang, B. Zhao, J. Hao, J. L. Luo and X. Z. Fu, *ChemSusChem*, 2020, **13**, 914–921.